New Journal of Physics
The open-access journal for physics

Micron-scale fast electron filaments and recirculation determined from rear-side optical emission in high-intensity laser–solid interactions

C Bellei[1,11], S R Nagel[1], S Kar[2], A Henig[3,4], S Kneip[1], C Palmer[1], A Sävert[5], L Willingale[1,7], D Carroll[8], B Dromey[2], J S Green[1,9], K Markey[2], P Simpson[2], R J Clarke[9], H Lowe[9], D Neely[9], C Spindloe[9], M Tolley[9], M C Kaluza[5,6], S P D Mangles[1], P McKenna[8], P A Norreys[1,9], J Schreiber[1,3,4], M Zepf[2], J R Davies[10], K Krushelnick[1,7] and Z Najmudin[1]

[1] Blackett Laboratory, Imperial College London, SW7 2AZ, UK
[2] Queen's University of Belfast, Belfast BT7 1NN, UK
[3] Max-Planck-Institut für Quantenoptik, Garching, Germany
[4] Department für Physik, Ludwig-Maximilians-Universität München, Garching, Germany
[5] Institut für Optik und Quantenelektronik, 07743 Jena, Germany
[6] Helmholtz-Institute Jena, 07743 Jena, Germany
[7] Center for Ultrafast Optical Science (CUOS), University of Michigan, Ann Arbor, MI 48109, USA
[8] University of Strathclyde, Glasgow G4 0NG, UK
[9] Central Laser Facility, STFC Rutherford Appleton Laboratory, Chilton, Oxon, OX11 0QX, UK
[10] GoLP, Instituto de Plasmas e Fusão Nuclear—Laboratório Associado, Instituto Superior Técnico, 1049-001 Lisboa, Portugal
E-mail: claudio.bellei05@imperial.ac.uk

New Journal of Physics **12** (2010) 073016 (12pp)
Received 10 March 2010
Published 21 July 2010
Online at http://www.njp.org/
doi:10.1088/1367-2630/12/7/073016

Abstract. The transport of relativistic electrons generated in the interaction of petawatt class lasers with solid targets has been studied through measurements of the second harmonic optical emission from their rear surface. The high degree of polarization of the emission indicates that it is predominantly optical transition

[11] Author to whom any correspondence should be addressed.

radiation (TR). A halo that surrounds the main region of emission is also polarized and is attributed to the effect of electron recirculation. The variation of the polarization state and intensity of radiation with the angle of observation indicates that the emission of TR is highly directional and provides evidence for the presence of μm-size filaments. A brief discussion on the possible causes of such a fine electron beam structure is given.

Contents

1. Introduction

The study of electron transport through dense plasmas is an active area of research of importance to many applications. Relativistic electrons generated in high-intensity laser–solid interactions can pass through the critical surface, where the laser energy is mostly absorbed, and continue, free from the influence of the laser, through to the rear surface of the target. The propagation of this large current of electrons can be affected by self-generated electric and magnetic fields, as well as collisions. A better understanding of this transport is a key issue for the success of the fast ignitor approach to inertial confinement fusion [1, 2] and may lead to optimization of ion acceleration from laser-irradiated solid targets [3, 4].

Electron transport has been studied by K_α and extreme ultraviolet (XUV) emission [5, 6], shadowgraphy [7]–[9] and optical emission [10, 11]. In particular, the divergence and temporal modulation of the electrons have been investigated by spatially and spectrally resolving rear-surface optical radiation [10]–[14]. This radiation can be attributed to thermal, synchrotron, transition radiation or coherent wake emission (CWE) [15].

These different mechanisms of emission can be distinguished by their polarization characteristics. Thermal (blackbody) radiation is not expected to be polarized. Synchrotron radiation (SR) is mainly polarized in the plane of motion of the electrons [16]. In our case it would be produced by electrons being pulled back by the electrostatic field that builds up at the back of the target [10], so that the polarization would vary across the emission region, depending on the direction in which electrons travel before restriking the surface. CWE is polarized in the plane of polarization of the laser field and is mainly emitted in the direction of propagation of the laser field [15]. Transition radiation (TR) is also polarized; its properties will be discussed in section 2.

In this paper, we present the first spatially resolved measurements of the polarization of the second harmonic optical emission from the rear of solid targets irradiated by high-intensity

lasers. The radiation is found to be uniformly polarized over the emission region, with a degree of polarization dependent on the orientation of the target rear surface, demonstrating that it is predominantly TR. The strong variation of the signal with the orientation of the target rear surface (or, in other words, of the angle of observation) reveals that, at high laser intensities, fast electrons propagate in micron-size filaments. Moreover, imaging the TR far from the laser axis gives direct evidence of the presence of recirculating currents.

This paper is organized as follows. The polarization and general properties of TR are briefly discussed in section 2. In section 3 we describe the results of two independent experiments, which were performed on the VULCAN CPA laser system at the Central Laser Facility. The results of section 3 are further discussed in section 4 and a brief summary of the paper is given in section 5.

2. Polarization properties of transition radiation (TR)

The total emitted energy of the TR per unit angular frequency and unit solid angle can be written as [17]

$$\frac{\mathrm{d}^2W}{\mathrm{d}\omega\,\mathrm{d}\Omega} = \frac{\mathrm{e}^2N}{\pi^2c}\left[\int \mathrm{d}^3\mathbf{p}\left(\mathcal{E}_\parallel^2+\mathcal{E}_\perp^2\right)+(N-1)\left(\left|\int \mathrm{d}^3\mathbf{p}\, g(\mathbf{p})\mathcal{E}_\parallel F\right|^2+\left|\int \mathrm{d}^3\mathbf{p}\, g(\mathbf{p})\mathcal{E}_\perp F\right|^2\right)\right], \tag{1}$$

where the first integral refers to the *incoherent* component of the transition radiation (ITR) and the second integral refers to the *coherent* one (CTR). Here, $g(\mathbf{p})$ is the momentum distribution function, $\mathcal{E}_\parallel$ and $\mathcal{E}_\perp$ are the Fourier transforms of the electric fields in the plane parallel and perpendicular to the radiation plane (defined by the directions of the target normal and the direction of observation) and F is a coherence function that takes into account the exact time and position at which electrons reach the interface.

Expressions for $\mathcal{E}_\parallel$ and $\mathcal{E}_\perp$ can be found in [18] for the case of two media with generic dielectric constant. However, for our purposes an interface that separates a perfect conductor from the vacuum can be assumed, in which case the Fourier fields simplify, becoming [17, 18]

$$\mathcal{E}_\parallel(\beta,\mu,u,\phi,\psi) = \frac{u\cos\psi[u\sin\psi\cos(\phi-\mu)-(1+u^2)^{1/2}\sin\beta]}{[(1+u^2)^{1/2}-u\sin\psi\cos(\phi-\mu)\sin\beta]^2-u^2\cos^2\psi\cos^2\beta}, \tag{2}$$

$$\mathcal{E}_\perp(\beta,\mu,u,\phi,\psi) = \frac{u^2\cos\psi\sin\psi\sin(\phi-\mu)\cos\beta}{[(1+u^2)^{1/2}-u\sin\psi\cos(\phi-\mu)\sin\beta]^2-u^2\cos^2\psi\cos^2\beta}, \tag{3}$$

where u is the normalized momentum, $u=\sqrt{\gamma^2-1}$, and all the other variables are shown in figure 1(a).

In the simplest case of a single particle traversing normal to a plasma–vacuum interface, TR is *radially* polarized, since $\mathcal{E}_\perp = 0$ for $\psi = 0$. In other words, the electric field oscillates in the radiation plane (figure 1(b)). For a particle that does not traverse normal to the interface the radiation is not radially polarized and a component normal to the radiation plane appears (figure 1(c)). In this general case, the polarization state is dependent on both the particle's momentum vector $\mathbf{p}$ and the direction of observation $\mathbf{k}$. Thus for a given set of observation angles the polarization state of the radiation carries information on the direction of the particles as they escaped the rear surface. This will be used for later considerations, to estimate the direction of the electrons from the polarization state of the radiation.

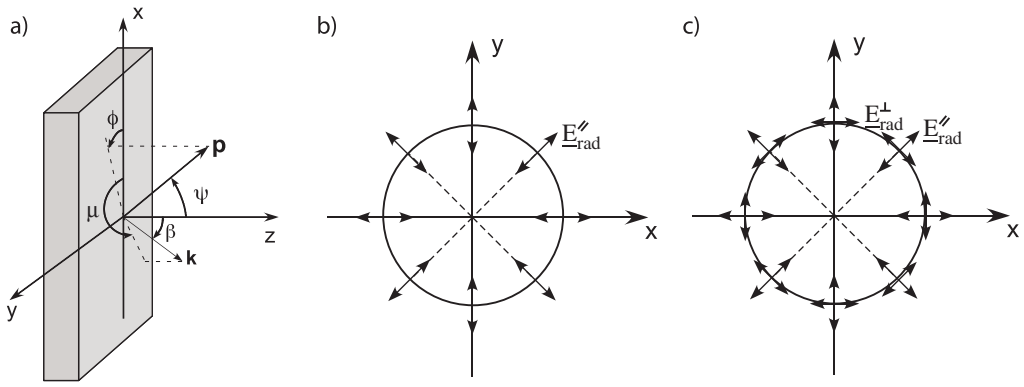

Figure 1. (a) Geometrical parameters involved in the calculations of TR. Here **p** is the particle's direction, **k** is the wave (observation) vector and z is the normal to the target rear surface. (b) For a charge crossing normal to the interface, the radiation is radially polarized. The magnetic field (not shown) is azimuthal. (c) In general, there is a component of the electric field parallel and normal to the radiation plane.

3. Experimental results

The experiments were performed with the VULCAN CPA laser operating with wavelength $\lambda_L = 1.054\,\mu$m and pulse length 580 ± 114 fs.

3.1. Experiment 1

A series of shots were taken with ~300 J of energy on target (experiment 1). The p-polarized laser pulses were focused by an $f/3$ parabola to a full-width at half-maximum (FWHM) spot size $w_0 \simeq 8\,\mu$m and a peak intensity $I \sim 10^{21}$ W cm^{-2} on to a range of flat Au foils of varying thickness at an angle of incidence of $\simeq 40^\circ$. The target rear surface was imaged at $\simeq 55^\circ$ from the target normal and $\simeq 15^\circ$ from the laser axis in the horizontal plane onto two 16-bit CCD cameras equipped with $2\omega_0$ interference filters and polarizers. The magnification was $\times 5$ with a theoretical resolution of 5 μm.

Figure 2(a) shows an image of the rear-surface emission from a 5 μm Au target. The image is horizontally polarized over the whole region. This is true for the extended halo as well as for the brightest central emission. Hence the emission is not thermal, and the uniformity of the polarization is also inconsistent with it being SR. The measurement is, however, consistent with it being radially polarized TR viewed in the horizontal plane.

The overall size of the emission region is larger than 200 μm. This can be partly justified by the fact that the prepulse acts so as to effectively increase the thickness of the target prior to the arrival of the main pulse. The presence of a prepulse can have significant effects on the physics of electron generation and proton acceleration [19, 20]. Measurements performed on the same laser system as in our experiment have shown that the distance from the critical surface for $\lambda_L = 1.054\,\mu$m to the initial target front surface is as high as 30 μm for the case of copper targets [21]. In these conditions and assuming that ballistic propagation applies, electrons would have to travel up to angles of 70° to the target normal in order to produce the emission region seen in the experiment.

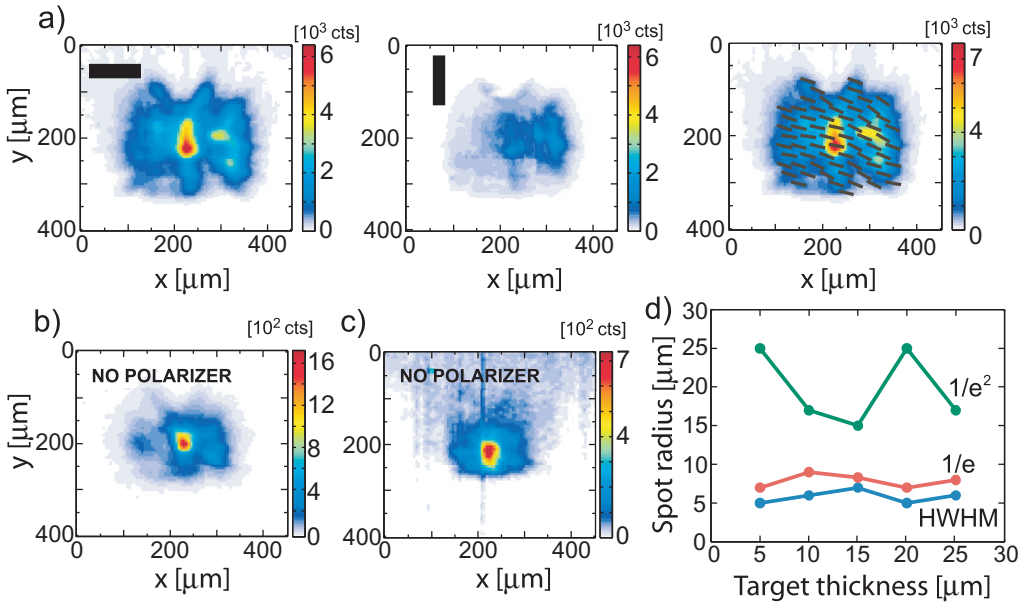

Figure 2. Experiment 1. Optical images at $2\omega_0$ for (a) 5 μm, (b) 15 μm and (c) 25 μm Au targets. (a) Left and central panels correspond to horizontal and vertical polarization, respectively, and the right panel is the resulting polarization map. (d) Radius of emission evaluated at $\frac{1}{2}$, $1/e$ and $1/e^2$ of the maximum intensity.

However, measurements of K_α and XUV radiation made on the same laser system and with comparable target thicknesses have shown that the overall beam size is limited to 80–130 μm [6], largely below our observations. Thus a likely explanation for this large emission area is that, while the bright central coherent transition radiation (CTR) emission is due to electrons escaping the target, the surrounding region is due to electrons refluxing at the target boundaries [22, 23]. Scattering and collisional losses should affect the propagation of these refluxing electrons that are therefore expected to emit incoherent radiation.

We also note that the CTR signal strength decreases with increasing target thickness, as expected, but the spatial extent of the emission remains relatively unchanged (figure 2(d)). For thicker targets (thickness $>100\,\mu$m), previous measurements have shown an increase in emission size with target thickness, consistently with the hypothesis of ballistic transport [10, 11].

3.2. Experiment 2

A further scan was performed on targets with varying rear-surface wedge angle. For these shots, an energy of up to 60 J on target was focused with $\simeq$35% of the energy within $w_0 \simeq 6\,\mu$m, to give $I \sim 8 \times 10^{19}\,\mathrm{W\,cm^{-2}}$. In this case the p-polarized pulses were incident at a fixed angle of 8° to the target normal.

The radiation was collected using an $f/3.5$ imaging system, centered at $\simeq$33° from the normal to the target front (i.e. $\simeq$41° to laser axis) in the horizontal plane, with magnification $\times$9.4 and theoretical resolution of 3 μm. The radiation was split into two orthogonal

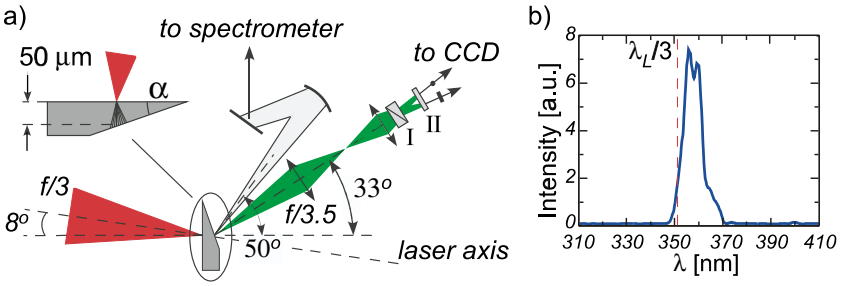

Figure 3. Experiment 2. (a) Experimental setup: I Wollaston prism and II $2\omega_0$ interference filter; α is the angle of the wedge. (b) Spectrum for $\alpha = 35°$, showing in detail the third harmonic.

polarizations with a Wollaston prism and imaged onto the same chip of a $2\omega_0$ filtered 16-bit CCD camera.

The radiation was also spectrally resolved from the NIR to the UV using an optical spectrometer with resolution ~1 nm. The harmonics of the laser frequency ω_0 were recorded in the emission, most strongly at $2\omega_0$, but also at $1\omega_0$, $3\omega_0$ and $4\omega_0$ (e.g. figure 3(b)). This supports the fact that the emission is mainly CTR at the harmonics of the laser frequency, indicating a combination of resonant and $\mathbf{j} \times \mathbf{B}$ heating [11].

Cu wedges with angles of $\alpha = 10°$, $20°$ and $35°$, as well as a 50 μm flat ($\alpha = 0°$) target, were used (figure 3(a)). The interaction point was chosen to ensure that the distance from the front to the rear surface was 50 μm for each target, thus keeping the effective foil thickness constant. The use of wedge targets allowed the angle that the fast electron beam formed to the rear surface to be varied without significantly changing the absorption at the front surface. Hence it can be assumed that the fast electrons produced in the interaction for all these targets had similar properties (temperature, direction, temporal envelope). As the collection optics were at a fixed position, this also enabled a variation of the angle of observation β, which is the angle between the rear side target normal and the direction of observation[12] (figure 1(a)).

In the following, two properties of the data collected in this campaign (experiment 2) will be discussed, as a function of the angle of observation β:

1. the polarization state of the radiation, from which an estimate for the *direction* of the electron filaments diagnosed by our imaging system will be inferred;
2. the integrated signal level recorded on the CCD camera, from which an estimate for the *size* of the electron filaments responsible for the CTR signal will be inferred.

3.2.1. Polarization data—direction of the electron filaments. The radiation exhibited a high degree of polarization that was dependent on the wedge angle α (figure 4). As for experiment 1, these images also exhibit a wide polarized halo surrounding the bright central CTR, most clearly seen in figure 4(c) for the case of the 10° wedge target. On the right side of this image, for both polarizations, a bright line of emission is seen from the target edge. This edge was not visible for the 20° and 35° wedge target, most likely because the filtering level had to be substantially increased due to the strong increase in signal level with α (see section 3.2.2). Both the extended

[12] Note that the angle of the wedge α and the angle of observation β only differ by a constant term, therefore in what follows they can be regarded as equivalent quantities.

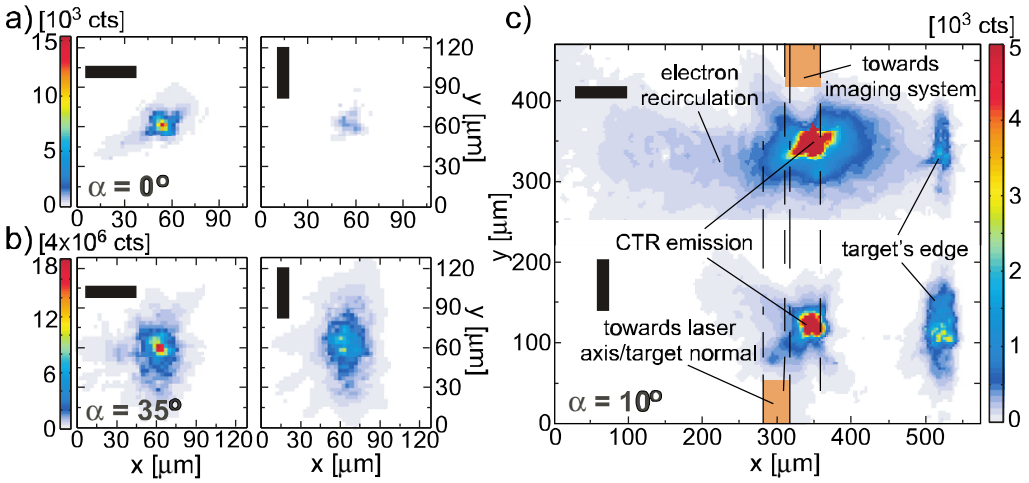

Figure 4. Experiment 2. Polarization analyzed images; lhs horizontal polarization and rhs vertical polarization for (a) 50 μm foil ($\alpha = 0^\circ$), (b) 35° wedge and (c) 10° wedge (here the top is horizontal polarization and the bottom is vertical polarization). The center is overexposed to enhance target visibility. Note that the peak intensity varied by more than three orders of magnitude from $\alpha = 0^\circ$ to 35°. The reason for this is clarified in section 3.2.2.

halo and the target-edge emission are at distances far from the initial interaction region in figure 4(c). Therefore, these effects can also be attributed to electron recirculation. *Ion emission* from the edge of solid targets has been observed previously [24], and has also been attributed to the dynamics of electrons transported through the targets by recirculation.

For flat targets the dominant polarization was horizontal, as before. However, increasing the wedge angle increased the relative contribution of the vertical polarization, as expected for TR.

A mean direction for the electrons diagnosed by our imaging system can be inferred from the dependence of the polarization state on the angle of observation β. Our choice has been to identify this polarization state by the ratio of the horizontal to the vertical polarization. For this analysis, the CTR component of equation (1) was integrated over the solid angle of the collection optics. The form factor F was evaluated, as shown in the next paragraph, 3.2.2; however, it is not of relevance for the present discussion. For each wedge target, the direction δ of a collimated beam of electrons was varied with respect to the *front* side target normal (which was not varied for the different wedge targets), as shown in the sketch of figure 5. For each of these directions, integration of equation (1) over the solid angle of the imaging system gives rise to a particular value of this polarization ratio. This process was then repeated for a different wedge target. Figure 5 shows the results for varying δ compared to the experimental results at different β (or, equivalently, α). The analysis suggests that the electron filaments diagnosed by the imaging system were directed within or close to the cone of the collection optics, i.e. $\delta \in [25^\circ, 42^\circ]$. This conclusion is also supported more directly by noting the distance of the main CTR from the laser axis in figure 4(c), which can be determined by measuring the distance from the target edge: the position of the CTR signal is within the cone of the first lens.

This result is expected, since for relativistic electrons the angular distribution of TR is confined to small angles along the particle's direction of propagation. The (theoretical) amount

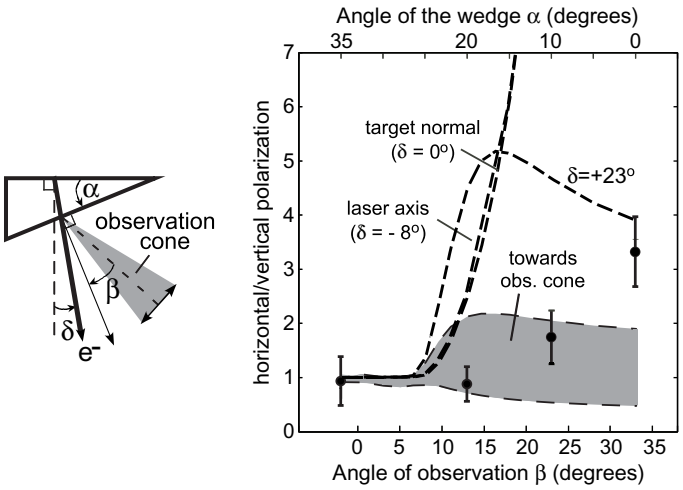

Figure 5. Experiment 2. Variation of the polarization ratio with observation angle β. Experiment (black circles) and theoretical predictions for different directions δ of electron beams (dashed lines). The shaded region is obtained assuming electrons directed within the observation cone of the imaging system, $\delta \in [25^\circ, 42^\circ]$. The relevant parameters are summarized in the sketch on the left.

of radiation collected by the imaging system as a function of δ, and for two different wedge targets ($\alpha = 0^\circ, 35^\circ$), is shown in figure 6. It is clear that electrons going towards the collection optics (denoted by the two vertical broken lines) are more easily detected by the imaging system. These plots are made assuming a Boltzmann momentum distribution for the fast electrons, with temperature T_e [17].

3.2.2. Signal intensity data—size of the electron filaments. The size of the main bright source of radiation in figure 4 is limited by the resolution of the imaging system. A measure of this size can also be obtained by using the angular distribution of the radiated energy, which for CTR should be strongly dependent on source size. Such an angular distribution was obtained from the intensity of the CTR for the different wedge targets.

To interpret the variation of the signal intensity with wedge angle, it is important to retain all the parameters in the CTR component of equation (1). In particular, the role of the form factor F is essential in this case. Physically, this term accounts for the phase difference of the waves emitted at the rear of the target. Therefore it depends on the time and position at which each electron reaches the back surface. Assuming that a train of impulsive electron bunches is produced at the front surface, that the beam is collimated and that the transverse profile of the electron beam is Gaussian, F is given by

$$F = G\frac{\sin(n_b\omega_{obs}\delta_T/2)}{\sin(\omega_{obs}\delta_T/2)}\exp\left[-\frac{1}{2}\left(\frac{\pi D_{2\sigma}}{\lambda_{obs}}\right)^2\sin^2\beta\right]. \quad (4)$$

Here, δ_T is the bunch period, n_b the number of bunches and $D_{2\sigma}$ the diameter of the beam at $1/\sqrt{e}$ maximum intensity. The effect of the quantity G (for which we do not give a full expression since it is not relevant for this discussion) is mainly a decrease in signal strength

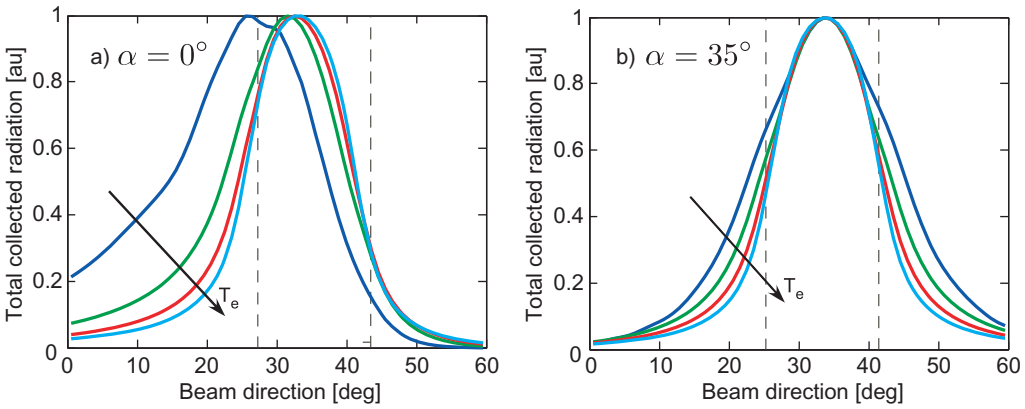

Figure 6. Total normalized energy collected by the imaging system as a function of the electron direction δ (measured with respect to the *front* side target normal, as in the sketch of figure 5), for (a) a flat target and (b) a 35° wedge target and for different electron temperatures (blue: 2 MeV, green: 5 MeV, red: 10 MeV, cyan: 20 MeV). The two broken lines mark the range of angles included in the cone of the first lens. Each curve is rescaled to its maximum value, in general more energy is radiated at higher temperatures.

with target thickness. The second term in equation (4) gives rise to harmonics of the bunch frequency in the spectrum, as reported previously [11, 13, 14].

The third term in equation (4) is the result of the Fourier transform of the transverse profile of the electron current [17, 25, 26]. It can be understood by analogy with classical diffraction in the far-field (Fraunhofer) approximation. The radiation emitted from the rear surface can be thought of as the diffraction of a plane wave by a circular aperture with a Gaussian transmission function. When the angle of observation β differs from zero, this term leads to a rapid decrease in intensity, depending on the transverse size of the beam $D_{2\sigma}$. This idea was suggested by Zheng *et al* [25] but, to our knowledge, in all previous experiments the observation angle was kept constant.

The data in figure 7 are consistent with this interpretation: the signal level varied by more than three orders of magnitude from the flat target ($\alpha = 0°$) to $\alpha = 35°$. The data have been fitted for different beam sizes. The electron temperature was assumed to be $T_e = 10$ MeV, but the dependence on T_e is weak. A best fit over all the experimental data implies an FWHM diameter $D = 1\,\mu$m[13] but the fall-off in signal strength at large β is too strong. A better fit is found if only the data for $\alpha = 0°$, 10° and 20° are considered. In this case, the best fit is for $D = 0.8\,\mu$m. For $D = 0.5\,\mu$m the calculated fall-off in signal would be slower than measured; for $D = 2.0\,\mu$m it would be too strong.

It is interesting to note that the inferred beam diameter is considerably smaller than the resolution of the imaging system, which was $\geqslant 3\,\mu$m. This might seem paradoxical; however, it is a simple application of Fourier optics: if the transmission function of the 'diffracting screen' is known and depends on one parameter only (the size of the aperture in this case), the knowledge of the angular distribution of the radiation is sufficient to determine the unknown parameter. The real advantage of imaging rather than using the angular distribution of the radiation is

[13] Note that for this discussion we refer to the FWHM diameter D rather than to $D_{2\sigma}$.

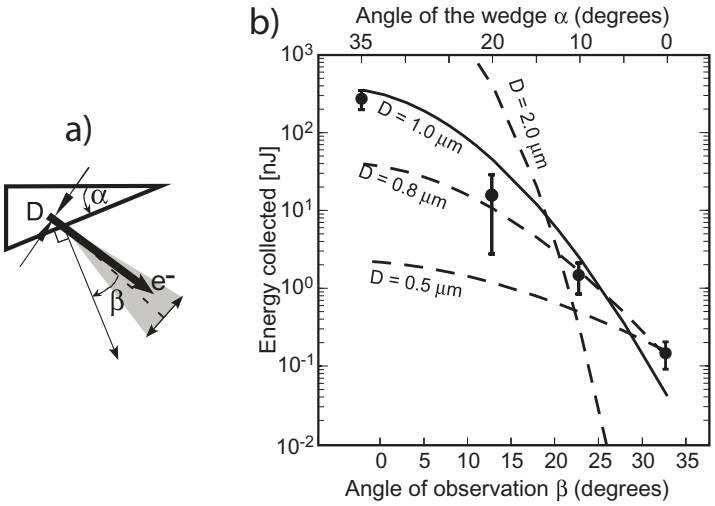

Figure 7. Experiment 2. Variation of signal intensity with β (angle between the center of the observation cone and the *rear* side target normal). Experimental (black circles) and theoretical fits (dashed lines, in arbitrary units) for different FWHM filament diameters D. The relevant parameters are summarized in the sketch on the left.

that in the former case no assumptions are made on the shape of the aperture, which is in fact directly measured. In our approach we assumed a Gaussian transmission function. As will be shown in the next section, when collisions are taken into account, this seems a reasonable assumption.

4. Discussion

An accurate modeling of the physics behind a laser–solid interaction at relativistic intensities is a complex task that has not been accomplished to date. It would not only require massive computational resources in order to resolve the Debye length, which is typically on the scale of nanometers at cold solid densities, but also require a significant step in understanding electron generation and transport through an initially cold solid material.

Despite this, a large number of simulation results are available in the literature, under some necessary simplifications, which demonstrate the formation of μm-scale filaments directed over a wide range of angles [27, 28]. Moreover, direct imaging of rear-surface emission has recently suggested the presence of filaments as small as 2 μm and with a mean size of 4 μm for intensities of $\sim 10^{19}\,\mathrm{W\,cm^{-2}}$ onto a range of different targets [29, 30]. Our results indicate that at higher intensities, the filament size can be below that observable with traditional imaging techniques.

However, in experiment 2 these filaments would have to propagate through $\simeq 50\,\mu$m of solid Cu, where angular scattering would be expected to cause rapid transverse expansion. Neglecting energy loss and assuming small total angular deflection, this 'beam blooming', defined as the variance of the transverse beam size due to scattering [31], can be written as

$$B \approx \frac{e^2}{2\sqrt{3\pi}\,\varepsilon_0} Z \sqrt{n_\mathrm{a} \ln \Lambda_s}\, \frac{s^{3/2}}{pv}, \tag{5}$$

where s is the distance traveled, Z the atomic number and n_a the atom number density; Λ_s is a term that depends on the electron–atom scattering cross section and p and v are the momentum and velocity of the electron, respectively. This result has been found to give excellent agreement with modeling using the Monte Carlo part of the code described in [32], where the angular scattering was found to lead to a Gaussian transverse density profile. Equation (5) shows that to obtain an FWHM ($\equiv 2\sqrt{2\ln 2}B$ for a Gaussian profile) smaller than 1 μm requires electrons with energies > 60 MeV, for all realistic values of Λ_s. Electrons with such high energies would be little affected by any plausible magnetic fields within the target.

However, this electron energy is well above the ponderomotive potential of the laser ($\simeq 4$ MeV) and an electron spectrometer placed along the laser axis in experiment 2 did not detect any electrons with energies above 30–40 MeV. Even though energy loss experienced by electrons in leaving the target could reduce this discrepancy, it appears that a simple interpretation of these results in terms of ballistic propagation, as has been used in the past, is not adequate. The influence of self-generated electric and magnetic fields inside the target, as well as collisions, should be considered. The results from the code LSP, which includes all of these effects, for parameters close to those of this experiment have shown no sign of filaments at 0.5 ps for intensities up to 10^{19} W cm^{-2}, but exhibit filaments 1–2 μm wide at 10^{20} W cm^{-2} (see figure 12 in [28]). In addition, resistive filamentation [33], rear-surface magnetic focusing [34] and instabilities associated with the electron sheath at the back surface may contribute to the observed small emission size.

5. Conclusions

In conclusion, we have presented the first polarization-resolved measurements of optical radiation emitted from the back of laser-illuminated solid targets and the first measurements of the effect of the angle of the back surface on this emission. The polarization allows us to identify the emission as principally CTR and not SR, CWE or thermal radiation. From the polarization properties of this radiation we have inferred the presence of electrons recirculating inside the target and deduced that the major contribution to the signal is due to electrons directed towards the imaging system. We have also shown that coherent TR can be used to directly characterize the source size with unprecedented spatial resolution, showing that it has an FWHM from 0.8 to 1 μm. Understanding the formation and behavior of these small-scale structures will be of vital importance for applications of high-intensity laser physics.

Acknowledgments

We acknowledge discussions with S Atzeni and R J Kingham and the assistance of the staff of the Central Laser Facility at the Rutherford Appleton Laboratory. MCK and AS thank the German Ministry of Education and Research (contract 03ZIK052) and the German Science Foundation (contract TR18) for support.

References

[1] Tabak M *et al* 1994 *Phys. Plasmas* **1** 1626
[2] Atzeni S 1999 *Phys. Plasmas* **6** 3316
[3] Clark E *et al* 2000 *Phys. Rev. Lett.* **84** 670

[4] Snavely R A *et al* 2000 *Phys. Rev. Lett.* **85** 2945
[5] Stephens R B *et al* 2004 *Phys. Rev.* E **69** 066414
[6] Lancaster K L *et al* 2007 *Phys. Rev. Lett.* **98** 125002
[7] Tatarakis M *et al* 1998 *Phys. Rev. Lett.* **81** 999
[8] Borghesi M *et al* 1999 *Phys. Rev. Lett.* **83** 4309
[9] Gremillet L *et al* 1999 *Phys. Rev. Lett.* **83** 5015
[10] Santos J J *et al* 2002 *Phys. Rev. Lett.* **89** 025001
[11] Baton S D *et al* 2003 *Phys. Rev. Lett.* **91** 105001
[12] Jung R *et al* 2005 *Phys. Rev. Lett.* **94** 195001
[13] Popescu H *et al* 2005 *Phys. Plasmas* **12** 063106
[14] Santos J J *et al* 2007 *Phys. Plasmas* **14** 103107
[15] Teubner U *et al* 2004 *Phys. Rev. Lett.* **92** 185001
[16] Jackson 1998 *Classical Electrodynamics* (New York: Wiley)
[17] Schroeder C B *et al* 2004 *Phys. Rev.* E **69** 016501
[18] Ter-Mikaelian M L 1972 *High-Energy Electromagnetic Processes in Condensed Media* (New York: Wiley-Interscience)
[19] MacPhee A G *et al* 2010 *Phys. Rev. Lett.* **104** 055002
[20] Kaluza M C *et al* 2004 *Phys. Rev. Lett.* **93** 045003
[21] Schreiber J *et al CLF Annual Report* 2008–2009, p 40
[22] Mackinnon A J *et al* 2002 *Phys. Rev. Lett.* **88** 215006
[23] Nilson P M *et al* 2009 *Phys. Rev.* E **79** 016406
[24] McKenna P *et al* 2007 *Phys. Rev. Lett.* **98** 145001
[25] Zheng J *et al* 2003 *Phys. Plasmas* **10** 2994
[26] Zheng J *et al* 2002 *Phys. Plasmas* **9** 3610
[27] Lasinski B F *et al* 1999 *Phys. Plasmas* **6** 2041
Ruhl H 2002 *Plasma Sources Sci. Technol.* **11** A154–8
Sentoku Y *et al* 2002 *Phys. Rev.* E **65** 046408
Ren C *et al* 2004 *Phys. Rev. Lett.* **93** 185004
Adam J C *et al* 2006 *Phys. Rev. Lett.* **97** 205006
[28] Evans R G 2006 *High Energy Density Phys.* **2** 35
[29] Storm M *et al* 2008 *Rev. Sci. Instrum.* **79** 10F503
[30] Storm M *et al* 2009 *Phys. Rev. Lett.* **102** 235004
[31] Li C K and Petrasso R D 2006 *Phys. Rev.* E **73** 016402
[32] Davies J R *et al* 1997 *Phys. Rev.* E **56** 7194
[33] Gremillet L *et al* 2002 *Phys. Plasmas* **9** 941
[34] Davies J R, Bell A R and Tatarakis M 1999 *Phys. Rev.* E **59** 6032